

**ICSV14**  
Cairns • Australia  
9-12 July, 2007



## **TRANSIENT VIBRATION ANALYSIS FOR GENERATING LOW ELECTRICAL POWER**

Mikail F. Lumentut <sup>a</sup>, Kian K. Teh <sup>b</sup> and Ian M. Howard <sup>b</sup>

<sup>a</sup> Research Student, Department of Mechanical Engineering, Curtin University of Technology, Australia

<sup>b</sup> Department of Mechanical Engineering, Curtin University of Technology, Australia

### **Abstract**

This paper presents a method for simulating low electrical power resulting from the transient vibration of a coupled piezosensor-plate structure using numerical finite element analysis. Love-Kirchhoff's plate theory, together with the piezoelectric constitutive equations were used to analyse the dynamic governing equations using the Lagrangian method. The piezoelectric direct mode effects generate polarity of the electric field due to an input transient force where the piezoelectric element was bonded onto the upper surface of the plate structure. Four node rectangular finite elements with twelve degrees of freedom per element were used for the coupled piezosensor-plate structure. The Newmark- $\beta$  numerical differential equation solution techniques were used within the MATLAB environment to simulate the resulting transient displacement and electric voltage responses. In this case, Rayleigh's proportional damping was used with damping constants chosen based on experimental results. The results obtained from the numerical modelling are compared with experimental work.

### **1. INTRODUCTION**

The use of piezoelectric materials for both sensor and actuator models includes many application areas in engineering including the well-known smart materials. Another concept is that of the smart structure, which includes coupling between the host structure and piezoelectric material.

Some mathematical models of smart materials and structures have been formulated using both numerical and finite element methods. Allik and Hughes [1] first formulated the numerical solution of piezoelectric material using finite element modelling. They developed the formulation of the three dimensional finite element model of the coupled field of the elastic-electric piezoelectric element using variational methods. Another model of the piezoelectric element has been discussed in detail by Naillon et al [2]. Moita, et al [3] developed coupling of the laminated plate and distributed piezoelectric sensor-actuators using finite element modelling and the Newmark method for the transient responses.

Some recent developments of piezoelectric technology concern the usage of sensors patched on the structure subject to ambient mechanical vibration. The induced strain energy can be converted to useful electrical energy capable of being stored on electrical devices such as batteries or capacitors which has become known as the energy harvesting technique with low power as discussed by Sodan et al [4]. Further study of the development of energy

harvesting has been discussed by Sodano et al [5], Amirtharajah & Chandrakasa [6] and Ottman et al [7].

In this paper, the coupled piezosensor and plate structure was investigated using numerical simulation of a finite element model to investigate the feasibility of energy harvesting. The theoretical model can be compared with experimental work in which the Newmark- $\beta$  algorithm was used to simulate the transient dynamic response and electric voltage time history. Moreover, the internal impedance of the piezoelectric element was investigated using a closed electric circuit under harmonic input force to optimise the maximum power harvested.

## 2. PIEZOELECTRIC CONSTITUTIVE EQUATIONS FOR POWER HARVESTING

Two modes of the piezoelectric effect can be formulated in the linear matrix equations relating the mechanical and electrical quantities as given by Tiersten [8],

$$\{\sigma\} = [C]\{\varepsilon\} - [e]^T \{E\}, \quad (1)$$

$$\{D\} = [e]\{\varepsilon\} + [\xi]\{E\}, \quad (2)$$

where  $\{\sigma\}$ ,  $\{D\}$ ,  $[e] = [d] [D_m]$ ,  $\{\varepsilon\}$ ,  $[\xi]$ ,  $[d]$ ,  $[D_m] = [C]$  and  $\{E\}$  represents the electric displacement vector, piezoelectric stress coefficient, strain vector, dielectric matrix at constant strain, piezoelectric constant, stiffness coefficient and electric field vector respectively. In this case the piezosensor has the direct mode capability of generating electrical energy, where the second term on the right hand side of Eq. (1) is neglected as it is smaller compared to the first term and the piezoactuator effect is not included in this case. The discretised electric field  $\{E\}$  creates polarisation in the piezosensor material, in the z-direction along the sensor plate thickness given by,

$$\{E\} = -\nabla\{\delta_{(z)}\} = -\nabla\{[\Phi_{(z)}^s]\{\delta_{(z)}^s\}\} = -[\Psi_{(z)}^s]\{\delta_{(z)}^s\}, \quad (3)$$

where  $\nabla$  is a gradient operator, the first derivative of the shape function with respect to thickness direction, giving,

$$[\Psi_{(z)}^s] = \begin{bmatrix} 0 & 0 & \frac{d\Phi_{(z)}^s}{dz} \end{bmatrix}^T = \begin{bmatrix} 0 & 0 & \frac{1}{t_s} \end{bmatrix}^T. \quad (4)$$

## 3. FINITE ELEMENT FORMULATION

According to classical plate theory with rectangular elements, the form of expression used in the solution was based on the non-conforming shape function as,

$$w(x, y) = [\Phi_n^{pl}(x, y)]\{\delta_n^{pl}(x, y)\}, \quad (5)$$

where  $[\Phi_n^{pl}(x, y)]$  is the shape function of the displacement field for the non-conforming function where the expression for the displacement term  $\{\delta_n^{pl}(x, y)\} \in \{\delta_i^{pl}(x, y), \delta_j^{pl}(x, y), \delta_k^{pl}(x, y), \delta_l^{pl}(x, y)\}$  and  $\forall \{w_n, \theta_{xn}, \theta_{yn}\}$  are the unknown vector forms for

each node. The shape function can be expanded by expressing the strain-displacement field of the element plate as follows,

$$\{\varepsilon\} = -z [\Psi_n^{pl}(x, y)] \{\delta_n^{pl}(x, y)\} \quad n \in \{i, j, k, l\}. \quad (6)$$

$[\Psi_n^{pl}(x, y)]$  is the differential matrix form of the strain-displacement relationship, given by,

$$[\Psi_n^{pl}(x, y)] = \left[ \frac{\partial^2 [\Phi_n^{pl}(x, y)]}{\partial x^2} \quad \frac{\partial^2 [\Phi_n^{pl}(x, y)]}{\partial y^2} \quad 2 \frac{\partial^2 [\Phi_n^{pl}(x, y)]}{\partial x \partial y} \right]^T \quad n \in \{i, j, k, l\}.$$

The plane stress field of the entire elements can be stated in the matrix form in equation (7) based on Equation (6) as,

$$\{\sigma\} = -z [D_{pl}] [\Psi_n^{pl}(x, y)] \{\delta_n^{pl}(x, y)\} \quad n \in \{i, j, k, l\}, \quad (7)$$

where;  $[D_{pl}]$  is the stiffness coefficient based on the material properties of both the piezoelectric and plate structure.

To obtain the dynamic equations of the smart structure, the compatible equations can be solved using Lagrange's formulation as;

$$\sum_{\eta=1}^s \left[ \frac{d}{dt} \frac{\partial \Pi}{\partial \dot{\delta}_\eta} - \frac{\partial \Pi}{\partial \delta_\eta} - F_\eta \right] = 0, \quad (8)$$

where :  $\forall \Pi = KE - PE + PEE$ ,  $\eta \in \left\{ \left\{ \dot{\delta}_n^{pl}(x, y) \right\}, \left\{ \delta_n^{pl}(x, y) \right\}, \left\{ \delta_{(z)}^s \right\} \right\}$ ,  $F_\eta \in \{ \{Fs\}, \{Fc\}, \{q\} \}$ ;

The generated energy,  $KE$  (Kinetic Energy),  $PE$  (Potential Energy) and  $PEE$  (Electrical Energy) and exerted work expressions can be accomplished by substituting Equations (1), (2), (3), (6) and (7) into each of the energy terms as required by equation (8). The results obtained from these calculations can be arranged in the following non-homogenous matrix differential equation, including Rayleigh damping as,

$$\begin{bmatrix} [M_{\phi\phi}^{pl}] & 0 \\ 0 & 0 \end{bmatrix} \begin{Bmatrix} \dot{\delta}_n^{pl}(x, y) \\ \delta_{(z)}^{se} \end{Bmatrix} + \begin{bmatrix} [C^{pl}] & 0 \\ 0 & 0 \end{bmatrix} \begin{Bmatrix} \dot{\delta}_n^{pl}(x, y) \\ \delta_{(z)}^{se} \end{Bmatrix} + \begin{bmatrix} [K_{\phi\phi}] & [K_{\phi\theta}] \\ [K_{\phi\theta}]^T & [K_{\theta\theta}] \end{bmatrix} \begin{Bmatrix} \delta_n^{pl}(x, y) \\ \delta_{(z)}^{se} \end{Bmatrix} = \begin{Bmatrix} F_\phi \\ F_\theta \end{Bmatrix}, \quad (9)$$

where:

$$[M_{\phi\phi}^{pl}] = \sum_{i=1} \left( \iiint \rho_i [\Phi_n^{pl}(x, y)]^T [\Phi_n^{pl}(x, y)] d(vol_i) \right), \quad [C^{pl}] = \alpha [M_{\phi\phi}^{pl}] + \theta [K_{\phi\phi}],$$

$$[K_{\phi\phi}] = \sum_{i=1} \left( z^2 \iiint [\Psi_n^{pl}(x, y)]^T [D_i] [\Psi_n^{pl}(x, y)] d(vol_i) \right),$$

$$[K_{\phi\theta}] = [K_{\theta\phi}]^T = - \sum_{se=1} \left( \frac{z}{2} \iiint [\Psi_n^{pl}(x, y)]^T [e]^T [\Psi_{(z)}^{se}] d(vol_{se}) \right), \quad [K_{\theta\theta}] = - \sum_{se=1} \left( \iiint [\Psi_{(z)}^{se}]^T [\xi] [\Psi_{(z)}^{se}] d(vol_{se}) \right),$$

and

$$\{F_\phi\} = \sum_{i=1} \left( \iint [\Phi_n^{pl}(x,y)]^T \{F_{s_i}\} d(area_i) + [\Phi_n^{pl}(x,y)]^T \{F_{c_i}\} \right), \quad \{F_\theta\} = - \sum_{i=1} \left( \iint [\Phi_{(z)}^{se}]^T \{q_i\} d(area_i) \right).$$

$\alpha$  and  $\theta$  are Rayleigh damping constants, that can be determined approximately through experimental methods. To obtain the eigenmodes, dynamic displacements and electric voltages, equation (9) can be solved using Guyan Reduction. At this point, the Newmark- $\beta$  algorithm was used to solve for the dynamic response of the piezo-plate vibration system.

#### 4. PZT ELECTRONIC CIRCUIT FOR ELECTRICAL POWER

To optimize the electrical power, a simple electronic circuit was used in the model. The voltage response of the PZT element under ambient vibration was AC voltage as discussed by Eggborn [9]. In this case, variable impedance from 0-15 k $\Omega$  was used to search for the matching PZT impedance as shown by the electronic circuit in Figure 2. The electrical voltage was measured by adjusting the variable impedance under harmonic response at the first plate resonance with an input force of 0.4 N to obtain the internal impedance of the PZT. The internal impedance of the PZT component was measured to be 3000  $\Omega$  where the maximum power was achieved by setting the variable impedance to be equal to the internal impedance of the PZT.

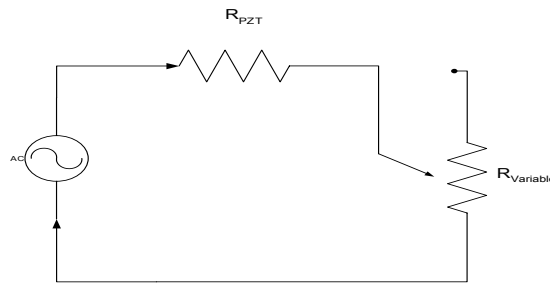


Figure 1. PZT electronic circuit for electrical voltage

#### 5. EXPERIMENTAL AND NUMERICAL COMPARISON

The material properties for the piezo-sensor and plate model were based on the PZT PSI-5A4E from Piezo Systems, INC. and steel material, respectively. The characteristics of the coupled piezo-sensor and plate material are given in table 1.

Table 1. Characteristic data

Item	Piezo-sensor	Plate
$E_C$ (GPA)	66	200
$\nu$	0.3	0.3
$\rho$ (kg/m <sup>3</sup> )	7800	7870
$t$ (m)	0.001	0.001
$d_{31}$ (m/V)	-190e-12	-
$d_{33}$ (m/V)	390e-12	-
$\xi_{33}$ (F/m)	1.602e-8	-
$l \times w$ (m <sup>2</sup> )	0.07467 x 0.07467	0.2964 x 0.21717

The experimental arrangement in Figure 2 shows a photograph taken of the experimental setup of the coupled piezo-plate structure with two-sided fixed-fixed support under transient force input. In addition, Figure 3 shows the structure model of the coupled piezo-plate.

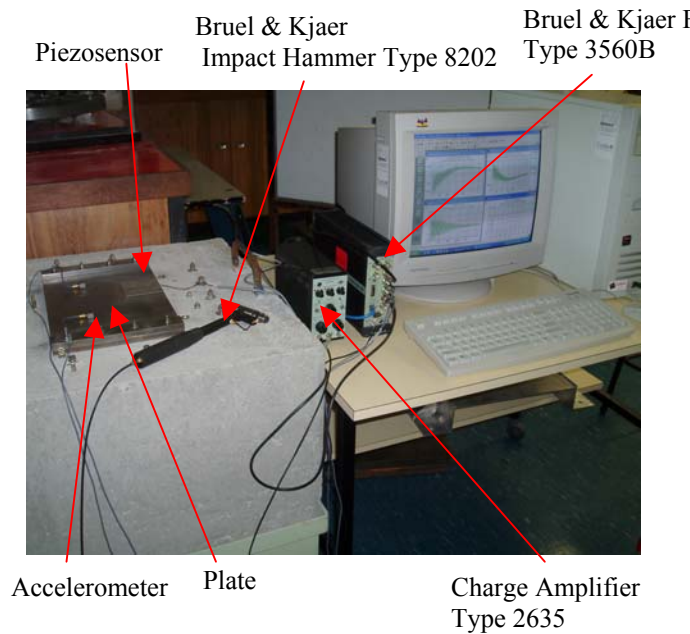


Figure 2. Experimental Setup of the Input Impact Force

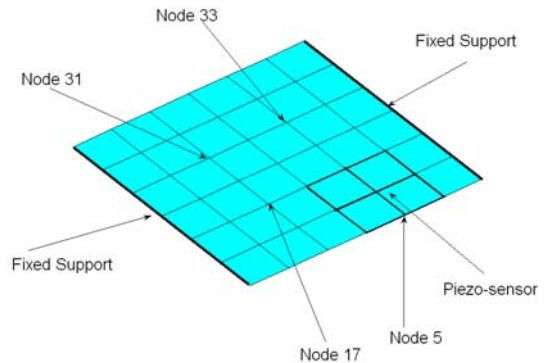


Figure. 3 Structure model using FEA of MATLAB Program

### 5.1 Dynamic Displacement Time History

The input force function was an impact of 2 N amplitude, experimentally generated using an impact hammer. The resulting plate dynamic displacement was then measured. Rayleigh's proportional damping constant multiplier ( $\alpha$ ) for the consistent mass matrix and proportional damping constant multiplier for the stiffness matrix ( $\theta$ ) were approximated based on the experimental results of  $6 \times 10^{-6}$  and  $2.15 \times 10^{-5}$ , respectively.

Figures 4a and 4b show the dynamic displacement time history of both numerical and measurement results at node 33. Both numerical and experimental results illustrated in Figure 4 show that several frequencies are present in the time waveform with the most dominant having a frequency close to 61 Hz, being the first resonance as shown in Figure 5. Furthermore, the maximum dynamic displacement from the numerical and measurement results gave values of 110  $\mu\text{m}$  and 112  $\mu\text{m}$ , respectively. As expected the transient response of the displacement time series tends to decay exponentially due to the internal damping of the structure. The dynamic displacement from the numerical analysis shows a smoother transient decay than that from the measurement. The displacement results were obtained by double integration of the acceleration measurement, which explains the slight offset and the low frequency variation in the results. The results obtained at nodes 33 indicated very similar response behaviour with just modest differences in displacement amplitude scale.

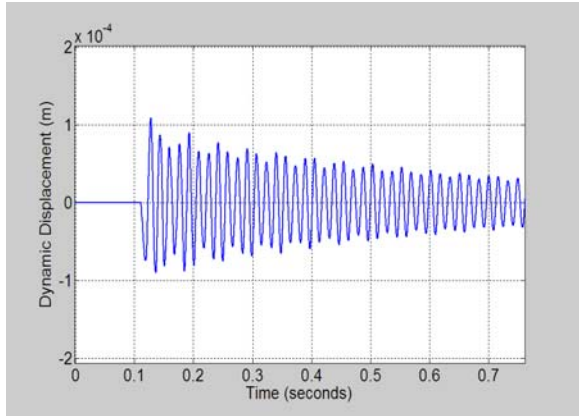


Figure 4a. Dynamic Displacement at Node 33 From Numerical Study

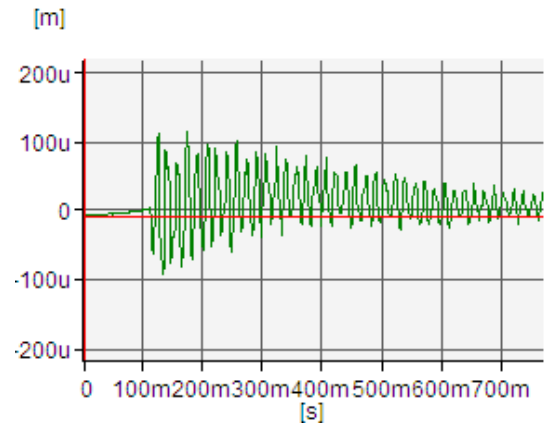


Figure 4b. Dynamic Displacement at Node 33 From Experimental Study

### 5.2. Coupled Piezo-Plate Dynamic Frequency Response

The dynamic frequency responses for the coupled piezo-plate structure were also obtained using numerical and measurement results. Figure 5 shows the numerical and experimental amplitude spectra obtained from the FFT (Fast Fourier Transform) at node 31 with input force of 2N at node 17. It can be seen that the first four resonance frequencies from numerical results are the dominant peaks corresponding to frequencies of 61.33 Hz, 80.44Hz, 169.6Hz and 177.7 Hz, respectively. The results obtained can be compared with the frequency response measurement from the FFT analyzer with values of 62.25 Hz, 85 Hz, 169 Hz and 181.6 Hz respectively. It can be seen that the measurement results gave a slight increase compared with the numerical results, with error percentages of 1.50 %, 5.67 %, 0.36% and 2.20 %, respectively. In this case, the comparison between numerical and experimental results in the FFT amplitude in dB (m) are very close with only modest discrepancies considering the limitation where the numerical model only used 36 elements (6x6).

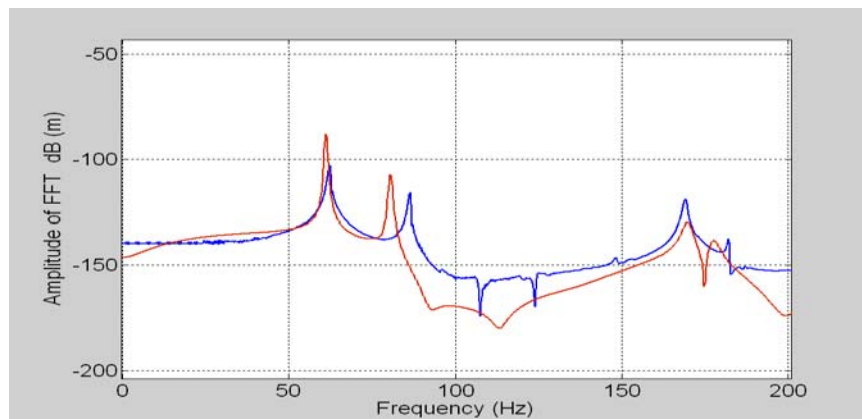


Figure 5. Frequency Response at Node 31 : FFT Amplitude (—) Numerical Study and (—)Experimental Study

### 5.3 Transient Electric Voltage Response

The electric voltage response obtained from a transient impact force was obtained from node 17 as shown at Figure 6. The numerical and experimental results are both shown for comparison. Figure 6a shows the electric voltage time history using the numerical result which gives a maximum voltage of 6.5 volt (downward) for the impact force between 0.11s to

0.13s by assuming a rectangular pulse force function of 2 N applied at 0.1s. After reaching the maximum voltage, the electric voltage gradually decays to zero. The measured electric voltage is shown in Figure 6b, with a maximum voltage measured to be 7.8 volt which then decays to zero. As shown in the numerical and experimental results, both reflect very similar amplitude response models by giving fairly small differences over the interval time. It also shows that the numerical result gave a smoother time waveform response compared with the experimental one. Repeated electric voltage responses can be obtained if the input force repeats periodically at certain time intervals.

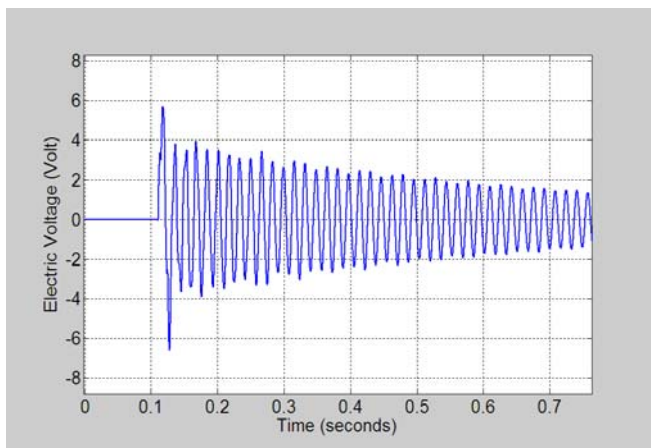


Figure 6a. Electric Voltage Time History From Numerical Study

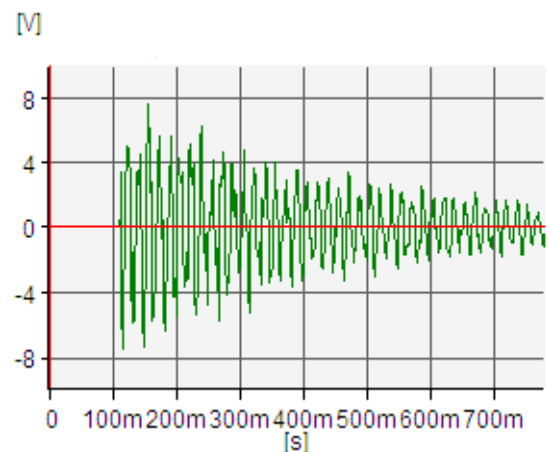


Figure 6b. Electric Voltage Time History From Experiment Study

#### 5.4 Low Power Harvesting from the Dynamic Response

This section analyses the low power harvesting that can be extracted from the piezosensor located at node 5 under ambient vibration conditions. In this case, the maximum electrical power harvested from the harmonic response can be calculated. The result obtained can be compared with the numerical method with a harmonic input force of 0.4 N. The internal impedance of 3000  $\Omega$  can also be used to analyse the power resulting from the transient response with the input force of 2 N.

It can be seen in Figure 7 that the maximum power versus impedance load from the numerical result occurs at 3000  $\Omega$  reaching to 40 mW using the previously shown closed circuit under harmonic response at the first resonance frequency of 61 Hz. As shown in Figure 7, from measurement the maximum power reached a peak value of 34 mW. The results shown in the two figures gave very similar power harvesting trends but a 6 mW difference was obtained in this case. The maximum electrical power obtained from the impact force transient response was also obtained from the numerical model and measurement. From the numerical model, the electrical power extracted from the piezosensor reached the value of 3.7 mW, as compared with the measurement which gave an increased value of 5.1 mW.

Overall, the electrical power from the piezosensor was investigated using numerical and measurement methods. The internal impedance was determined from the first resonance by measurement when the electric voltage gave the highest value. The result obtained from power harvesting has an inevitable limitation. The reason for this case is the use of the simple electronic circuit to predict the internal impedance of the piezoelectric element bounded on the plate structure.

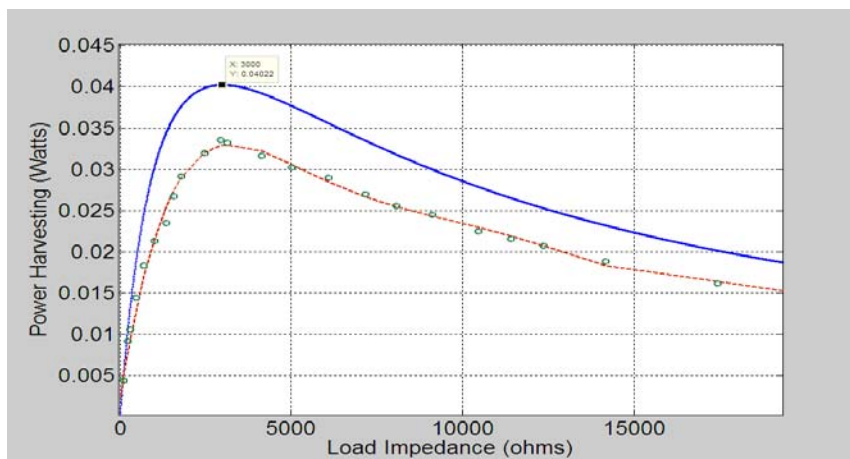


Figure 7. Power Harvesting Versus Load Impedance at First Resonance Frequency : Numerical Study (—) and Experimental Results (---)

## 6. CONCLUSION

The transient vibration simulation of a smart structure for generating power using finite element analysis has been presented. The constitutive equations of the piezoelectric element coupled with the Love-Kirchhoff's plate were modelled to formulate the finite element model focusing on the numerical transient response obtained using the Newmark- $\beta$  algorithm. The numerical model was investigated using the coupled field finite element model simulated using the MATLAB program. The investigation of internal impedance was taken into consideration to model the simple closed electric circuit for the measured power. The results obtained from the dynamic displacement, electric voltage and power harvested under impact force using numerical and experimental models showed very similar trends in dynamic response with small differences in amplitudes. The electronic circuit design should be further developed to obtain more accurate results of electrical power.

## REFERENCES

- [1] Allik, H & Hughes, T.J.R. (1970). "Finite Element Method for Piezoelectric Vibration", *International Journal for Numerical Methods in Engineering*, Vol. 2, No. 2, pp.151-157.
- [2] Naillon, M., Coursant R.H. & Besnier, F. (1983). "Analysis of Piezoelectric Structures by a Finite Element Method." *ACTA Electronica*, Vol. 25, No. 4, pp. 341-362.
- [3] Moita, J. M., Correia, I.F.P. & Soares, C.M.M (2004). "Active Control of Adaptive Laminated Structures with Bounded Piezoelectric Sensors and Actuators", *Computer & Structures*, Vol. 82, pp. 1349-1358.
- [4] Sodano, H. A., Inman, D.J. & Park, G. (2004). "A Review of Power Harvesting from Vibration Using Piezoelectric Materials", *The Shock and Vibration Digest*, Vol. 36, No. 3, pp. 197-205.
- [5] Sodano. H.A., Inman, D.J. and Park. G. (2005). "Comparison of Piezoelectric Energy Harvesting Devices for Recharging Batteries", *Journal of Intelligent Material Systems and Structures*, Vol. 16. pp. 799-807.
- [6] Amirtharajah, R. & Chandrakasa, A.P. (1998). "Self-Powered Signal Processing Using Vibration-Based Power Generation", *IEEE Journal of Solid-State Circuits*, Vol. 33, No. 5, pp.687-695.
- [7] Ottman, G. K., Hofmann, H.F. & Lesieutre, G.A. (2003). "Optimized Piezoelectric Energy Harvesting Circuit Using Step-Down Converter in Discontinuous Conduction Mode", *IEEE Transactions on Power Electronics*, Vol.18, No. 2, pp. 696-703.
- [8] Tiersten, H.F. (1969), "Linear Piezoelectric Plate Vibrations", *Plenum Press*.
- [9] Eggborn, T. (2003). "Analytical Models to predict Power Harvesting with Piezoelectric Materials", *Master Thesis*, Virginia Polytechnic Institute and State University, Virginia.